PLOS NEGLECTED TROPICAL DISEASES

RESEARCH ARTICLE

Therapeutic and antioxidant potential of bionanofactory *Ochrobactrum sp*.-mediated magnetite and zerovalent iron nanoparticles against acute experimental toxoplasmosis

Nehal Nassef Hezema[1], Marwa Moustafa Eltarahony[2]*, Sara Ahmed Abdel Salam[1]*

1 Department of Medical Parasitology, Faculty of Medicine, Alexandria University, Alexandria, Egypt, **2** Department of Environmental Biotechnology, Genetic Engineering and Biotechnology Research Institute, City of Scientific Research and Technological Applications, New Borg El-Arab City, Alexandria, Egypt

* m_eltarahony@yahoo.com (MME); sara.abdelsalam@alexmed.edu.eg, sara_cielbleu@msn.com (SAAS)

Citation: Hezema NN, Eltarahony MM, Abdel Salam SA (2023) Therapeutic and antioxidant potential of bionanofactory *Ochrobactrum sp.*-mediated magnetite and zerovalent iron nanoparticles against acute experimental toxoplasmosis. PLoS Negl Trop Dis 17(10): e0011655. https://doi.org/10.1371/journal.pntd.0011655

Editor: Travis J. Bourret, Creighton University, UNITED STATES

Received: May 4, 2023

Accepted: September 11, 2023

Published: October 6, 2023

Data Availability Statement: All data underlying our findings are described in manuscript and uploaded as supplementary information.

Funding: The author(s) received no specific funding for this work.

Competing interests: The authors have declared that no competing interests exist.

Abstract

The control of toxoplasmosis, a rampant one health disease, has been focussed on conventional antitoxoplasmic agents with their adverse outcomes, including serious side effects, treatment failure and emergence of drug resistant strains. Nanobiotechnology may provide a strong impetus for versatile alternative therapies against toxoplasmosis. Bionanofactory *Ochrobactrum sp*. strain CNE2 was recruited for the biosynthesis of functionalized magnetite iron nanoparticles (MNPs) and nanozerovalent iron (nZVI) under aerobic and anaerobic conditions and their therapeutic efficacy was evaluated against acute toxoplasmosis in murine model. The formation of self-functionalized spherical nanoparticles varied in size, identity and surface properties were substantiated. Mice were orally administered 20 mg/kg of each formulation on the initial day of infection and continued for seven consecutive days post infection (PI). Parasitological, ultrastructural, immunological, and biochemical studies were performed for assessment of therapeutic activity of biogenic iron nanoparticles (INPs). Parasitologically, MNPs showed the highest antitoxoplasmic efficacy in terms of 96.82% and 91.87% reduction in mean tachyzoite count in peritoneal fluid and liver impression smears, respectively. Lesser percentage reductions were recorded in nZVI-treated infected subgroup (75.44% and 69.04%). In addition, scanning electron microscopy (SEM) examination revealed remarkable reduction in size and extensive damage to the surface of MNPs-treated tachyzoites. MNPs-treated infected mice revealed a statistically significant increase in the serum levels of both interferon gamma (IFN-γ) to 346.2 ± 4.6 pg/ml and reduced glutathione (GSH) to 8.83 ± 0.30 mg/dl that subsequently exerted malondialdehyde (MDA) quenching action. MNPs showed a superior promising antitoxoplasmic activity with respect to both spiramycin (SPI) and nZVI. To best of our knowledge, this is the first study of a biosafe oral iron nanotherapeutic agent fabricated via an eco-friendly approach that offers promising potential against acute experimental toxoplasmosis.

Author summary

Toxoplasmosis is transmitted via food, water, and blood-borne zoonosis caused by an obligate intracellular parasite, *Toxoplasma gondii* (*T*. *gondii*). The opportunistic nature and distinct ability of *T*. *gondii* to inhabit almost all nucleated cells of any warm-blooded host makes it an important global public and animal health concern. Toxoplasmosis, a major neglected tropical disease, may lead to a devastating disease especially among immunocompromised patients and infants born to infected mothers. The emergence of resistant strains and development of serious side effects of the gold standard treatment, pyrimethamine and sulfadiazine, deemed as major causes of treatment failure. Besides, these drugs cannot be used during pregnancy because of the deleterious effects on the fetal development. Consequently, the present work focused on utilization of biologically-synthesized iron nanoparticles (INPs) that can cross cell membranes and reach specific targets more easily than multiple drugs. INPs were biosynthesized by an eco-friendly approach under aerobic and anaerobic conditions. Orally administered INPs displayed significant antioxidant and antitoxoplasmic activity and afforded high levels of safety in mice. Collectively, the marked therapeutic activity and the safe nature of biosynthesized INPs enable them to serve as a promising nanotherapeutic antitoxoplasmic agents.

Introduction

Toxoplasmosis is a ubiquitous one health disease that affects not only the health of human, domestic and wildlife animals but also the ecosystems [1]. It is caused by the opportunistic parasite, *Toxoplasma gondii* (*T*. *gondii*), that exhibits heteroxenous life cycle comprising felines as definitive hosts and homeotherms (rodents and humans) as intermediate hosts [2]. Man contacts the infection by accidental ingestion of oocysts in contaminated food and water, tissue cysts in improperly cooked meat or tachyzoites in unpasteurized milk [3]. Moreover, toxoplasmosis can be transmitted via blood transfusion, organ transplants or vertical transmission [4]. Although, 90% of infected individuals are asymptomatic, newborns and immunocompromised patients may present with serious health problems [4].

To date, the combination of pyrimethamine, sulphonamides and folinic acid is the gold standard treatment for toxoplasmosis [5]. However, pyrimethamine-related myelosuppression and hypersensitivity reactions to sulphonamides were reported [6,7]. Spiramycin (SPI), azithromycin, clarithromycin, atovaquone, and cotrimoxazole, have been found to be effective in treatment of toxoplasmosis [4]. The reported treatment failures of the current licensed drugs may be related to poor compliance (long-term treatment and drug intolerance) or emergence of drug-resistant strains [8]. To overcome this forthcoming alarming situation, the need for novel, facile yet selective therapeutics against toxoplasmosis is an eternal challenge.

Metal-based nanoparticles (NPs) have unprecedentedly revolutionized research in parasitology, owing to their unique physico-chemical properties [9]. Besides antitoxoplasma potential of chemically synthesized metal NPs [10,11], biogenic metal NPs as silver [12], selenium [13], zinc [14] and copper [15] had shown a considerable antitoxoplasmic activity. Iron is an essential micronutrient that plays a vital role in cellular functions of versatile prokaryotic and eukaryotic cells [16,17]. A large body of evidence supports the high reactivity and biocompatibility of iron-based nanoparticles (INPs) as compared to other noble metals such as gold and silver [18]. Microbial synthesis of INPs, is an eco-friendly approach that converts iron (Fe) ions into nanoscale iron particles using enzymes and versatile secondary metabolites [19].

Among INPs, magnetite iron nanoparticles (MNPs) and nanozerovalent iron (nZVI), have been extensively investigated in treatment of infectious diseases.

Magnetite-based NPs, iron oxide NPs, are preferred in biomedicine due to their biocompatibility, superparamagnetic and biodegradable properties [20]. Some MNPs formulations are approved by Food and Drug Administration for their use in treatment of iron deficiency anemia and as magnetic resonance imaging contrast agents [21]. Apart from the advances witnessed in cancer therapeutics, green-synthesized MNPs have been exploited against various pathogenic strains of bacteria and fungi [22,23,24]. Concerning parasites, a recent *in vivo* study had reported an enhanced activity of biogenic MNPs against *Schistosoma mansoni* (*S. mansoni*) [25].

nZVI, a composite consisting of Fe (0) core and ferric oxide coating, has the potential to interact with pollutants in the environment and influence the living organisms [26,27]. Besides remediation of environment, green-synthesized nZVI possesses anti-cancer [28], antibacterial [29,30], antifungal [30], and antischistosomal activities [25].

With such a multitude of applications of green-synthesized MNPs and nZVI, they proved their potential as effective anti-schistosomal agents [25]. Leaping the hurdles in developing treatments for toxoplasmosis, the potential antiparasitic activity of these biogenic INPs is worth to be studied. Accordingly, the objective of the current study was to evaluate the therapeutic and antioxidant potential of biogenic MNPs and nZVI against acute experimental toxoplasmosis. The therapeutic activity of biosynthesized NPS was assessed using parasitological, ultrastructural, immunological and biochemical studies against acute toxoplasmosis in a murine model.

Materials and methods

I. Ethics statement

Following the Egyptian national regulations for laboratory animal experimentation, the experimental protocol was approved by the Ethics Committee of the Faculty of Medicine, Alexandria University, Egypt (Protocol approval number: 0305745).

II. Animals

Four to six-week-old male Swiss strain albino mice, weighing 20–25 grams, were obtained from the animal house of the Medical Parasitology Department, Faculty of Medicine, Alexandria University, Egypt. Mice were kept in a suitable healthy rearing environment with standard conditions of light and temperature as well as free access to food and water.

III. *T. gondii* strain and infection

The Virulent RH HXGPRT (-) strain of *T. gondii* was maintained in the laboratory of the Medical Parasitology Department, Faculty of Medicine, Alexandria University, Egypt, by serial intraperitoneal (IP) passage of tachyzoites in Swiss strain albino mice every five days [31]. For animal infection, tachyzoites were harvested from peritoneal exudates of infected mice. Then, the tachyzoites were counted by the haemocytometer and injected intraperitoneally at a dose of 2500 tachyzoites/100 μl saline per mouse for induction of acute infection model [32].

IV. Drugs

Spiramycin (3 M.I.U.) was purchased from local pharmacy. Each tablet was weighed, crushed and dissolved in phosphate buffer saline (PBS). It was given to mice orally at a dose of 400 mg/kg once daily [33].

MNPs and nZVI were biosynthesized in the laboratory of City of Scientific Research and Technological Applications, Alexandria, Egypt. A pilot study was conducted to determine the lowest effective oral dose of MNPs and nZVI capable of decreasing the total tachyzoites burden, and 20 mg/kg/day was selected.

V. Biosynthesis and characterization of MNPs and nZVI

The bacterial strain, *Ochrobactrum sp*. *CNE2*, was isolated from a freshwater sample collected from Mahmoudia canal, Alexandria, Egypt. The strain *CNE2* was identified by 16S rDNA sequencing as *Ochrobactrum sp*. *CNE2* strain and its gene sequence was deposited in the GenBank under the accession number of MN631047. On optimized production medium, the bacterial inoculum of 0.5 McFarland (approximately 10^8 CFU/mL) was cultivated and incubated aerobically and anaerobically according to detailed protocol described by Zaki *et al.* [34]. After complete incubation, the bacterial biomass containing INPs was harvested, washed and INPs were extracted, washed, dried and subjected for further characterization.

The optical features with related surface plasmon resonance (SPR), crystalline phase, particle's identity, purity, and morphological properties of both biosynthesized INPs were determined through a Labomed model UV-Vis double-beam Spectrophotometer, X-ray diffractometer (XRD) (Shimadzu 7000, USA), and transmission electron microscopy (TEM) (JEOL JEM-1230), respectively. Whereas, the analysis of elemental constituents and functional groups was performed by energy dispersive X-ray spectroscopy (EDX) (JEOL JSM-6360LA) and Fourier-transform infrared spectroscopy (FTIR) (Shimadzu FT-IR-8400 S, Japan), respectively. The surface charge, overall INPs size distribution profile in aqueous solution, poly dispersity index (PDI) and their zeta potential (ZP) were assessed using a zeta sizer (Malvern Instrument ZS-Nano, UK) [35].

VI. Animal grouping and experimental design

Forty-eight mice were divided into 24 serving as non infected group (I) and 24 as infected group (II). Group I was further subdivided into 4 equal subgroups as follows: Subgroup Ia, Non infected non treated; Subgroup Ib, Non infected SPI-treated; Subgroup Ic, Non infected MNPs-treated; and Subgroup Id, Non infected nZVI-treated. Group II was subdivided into 4 equal subgroups as follows; Subgroup IIa, Infected non treated; Subgroup IIb, Infected SPI-treated; Subgroup IIc, Infected MNPs-treated; and Subgroup IId, Infected nZVI- treated.

The dose of the treating drugs was calculated and suspended in 100 μl of PBS per mouse. 100 μl of PBS were orally administrated to mice of the non treated subgroups (Ia and IIa) in the same schedule as treated subgroups. Treatment was initiated on the same day of infection and continued for seven consecutive days. Mice of Group II were infected intraperitoneally with 2500 tachyzoites/100 μl saline per mouse. Animals of all subgroups were sacrificed on the 8^{th} day post infection (PI) for assessment of efficacy of therapy.

VII. Parasitological study

VII.1. Mortality rate. The mortality rate (MR) was estimated at the time of sacrifice on 8^{th} day PI in treated subgroups (Ib, Ic, Id and IIb, IIc, IId) and compared with their corresponding non treated subgroups (Ia and IIa), respectively [36]. The MR% for each subgroup was assessed by the following equation:

$$\mathrm{MR}\ (\%) = \frac{\text{Number of dead mice on the day of sacrifice}}{\text{Number of mice at the beginning of the experiment}} \times 100$$

VII.2. Parasite count. Parasite burden was estimated on the day of sacrifice by counting the extracellular tachyzoites in the peritoneal fluid (per ml) using a hemocytometer as well as in ten high power fields of Giemsa-stained impression smears of liver of each infected mouse [33,36]. Then, the mean number of tachyzoites in each infected subgroup was calculated. The percentage reduction (%R) in the parasite burden, whether in peritoneal fluid or liver impression smears, was calculated according to the following equation: [37]

$$\text{Percentage reduction (\%R)} = \frac{N - n}{N} \times 100$$

N: Mean tachyzoite count recovered from the infected non treated control subgroup
n: Mean tachyzoite count recovered from each infected treated subgroup

VIII. Ultrastructural study

Tachyzoites harvested from the peritoneal fluid of mice in the infected subgroups were fixed in cold 2.5% buffered glutaraldehyde phosphate, dehydrated using an ascending series of ethanol and examined under scanning electron microscopy (SEM) (JEOL JSM, IT200, Japan) [38].

IX. Immunological and biochemical studies

Blood samples were collected by cervical incision of each mouse on the 8th day PI. They were centrifuged and serum samples were separated and kept at -20˚C to be used for the immunological and biochemical studies.

IX.1. Immunological study. The level of IFN-γ was measured in the sera of mice of all subgroups using commercial mouse interferon gamma (IFN-γ) ELISA kit (Chongqing Biospes, China). The assay was carried out according to the manufacturer's protocol. The detection range of the kit was 31.2–2000 pg/ml.

IX.2. Biochemical study. *IX.2.1. Oxidative stress*. Reduced glutathione (GSH) and malondialdehyde (MDA) levels were determined colorimetrically in the sera of mice in all subgroups using commercial kit (Biodiagnostics, Egypt) according to the manufacturer's instructions.

IX.2.2. Toxicity. Sera from mice in the non infected treated subgroups (Ib, Ic and Id) were used to reveal any toxic effect of the treating drugs on liver and kidney functions in comparison to the non-infected non treated subgroup (Ia). Double enzymatic reaction method was used to measure liver enzymes; aspartate transaminase (AST) and alanine transaminase (ALT). While kidney function tests (serum urea and creatinine) were measured by Jaffe reaction method [39].

X. Statistical analysis of the data

Data were fed to the computer and analyzed using IBM SPSS software package version 20.0. (IBM Corp, Armonk, NY, USA). For continuous data, Shapiro-Wilk test was used to verify the normality of distribution of variables. Quantitative data were described using range (minimum and maximum), mean, standard deviation and median. One way ANOVA test (F-test) was used for normally distributed quantitative variables, to compare between more than two groups, followed by Tukey's *post Hoc* test for pairwise comparison. Significance of the obtained results was judged at the 5% level (p value ≤ 0.05).

Results

I. Characterization of MNPs and nZVI

I.1. Visual and optical properties. The present study sought the eco-friendly fabrication of INPs by *Ochrobactrum sp*. strain CNE2 under nitrate utilization aerobically and

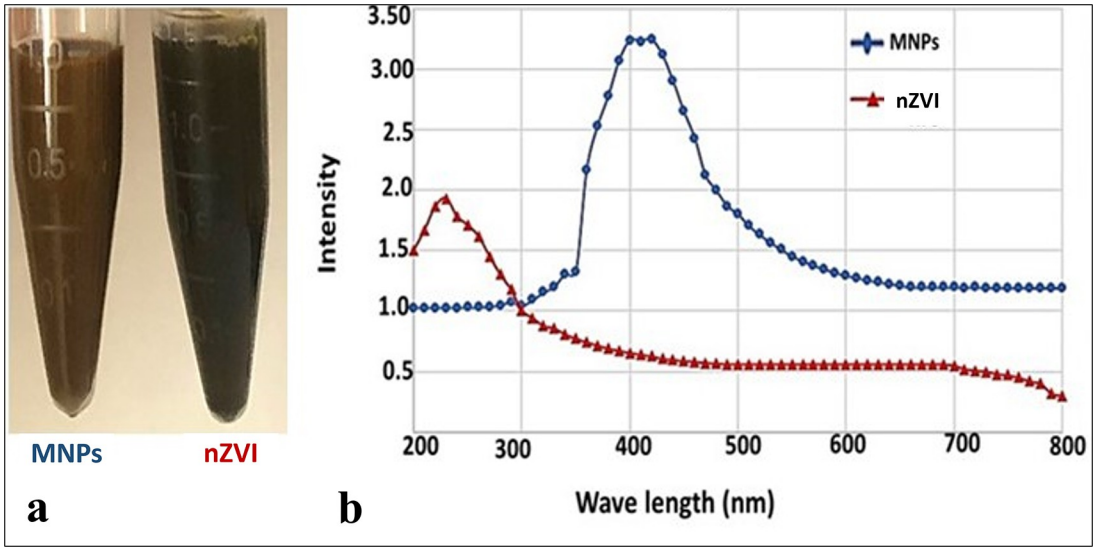

Fig 1. Visual (a) and optical properties (b) of INPs.

https://doi.org/10.1371/journal.pntd.0011655.g001

anaerobically. Colour changes in the bacterial biomass and its ambient milieu from pale yellow to deep brown/black were affirmed and confirmed by UV-Vis spectrophotometer comparing to the control trials (Fig 1A). The SPR, showed the appearance of single, symmetric, sharp absorption peaks with no tailing at 419 and 233 nm for MNPs and nZVI, respectively (Fig 1B). In agreement with our results, Puthukkara *et al.* [40], stated that the range of 210 to 240 nm in UV-Vis spectra consider being a reliable indicator for the presence of metallic INPs. On the other hand, Mahdavi *et al.* [41], showed that magnetite NPs prepared by *Sargassum muticum* aqueous extract exhibited SPR at 415 nm.

I.2. Structural properties. The diffractogram of aerobically synthesized MNPs displayed a series of characteristic peaks at 2θ = 30.9˚ (220), 35.6˚ (311), 43.8˚ (400), 54.5˚ (422), 57˚ (511), 63.5˚ (440) and 74.5˚ (533); unraveling the formation of orthorhombic phase MNPs (JCPDS no:19–0629) (Fig 2A). However, the anaerobically synthesized nZVI showed two peaks at 2θ = 44.73˚ and 64.81˚, which correspond to Bragg's reflection values of (110) and (200), respectively. The reflection peaks position and their relative intensities pointed out that the anaerobically synthesized INPs were nZVI and match those of the standard spectrum (JCPDS no: 01-085-1410). Notably, small peak was observed at 2θ = 36.11˚, which corresponds to (111) plane of FeO (JCPDS no: 772355) (Fig 2B). The presence of this peak in low intensity revealed the oxidation of nZVI surface during extraction, washing and processing step, which agreed with the results obtained by chemical and phyco-synthesis methods [42]. Undoubtedly, the presence of sharp and obviously distinguished peaks in XRD diffractograms of both aerobically and anaerobically synthesized INPs indicated the crystalline nature of them with the lowest surface energy [43].

The elemental profile of MNPs prepared aerobically by strain CNE2 confirmed that iron and oxygen were the major ingredients in the examined material. The iron main peaks were noticed at binding energies of 0.8, 6.3 and 7.0 keV with atomic percentages of 57.11%; a remarkable signal at 0.5 KeV with atomic percentage of 29.75% was identified for oxygen (Fig 2C). While predominant peak was observed at range of 6–7 keV with atomic percentages of 77.3% that is related to iron binding energy in nZVI sample (Fig 2D). Additional small peak was observed in anaerobically synthesized nZVI at binding energy of oxygen (0.5 keV) with atomic percentages of 1.5% (Fig 2D). In addition, the peaks closer to 0.27, 0.3, 2.0 and 2.3 keV

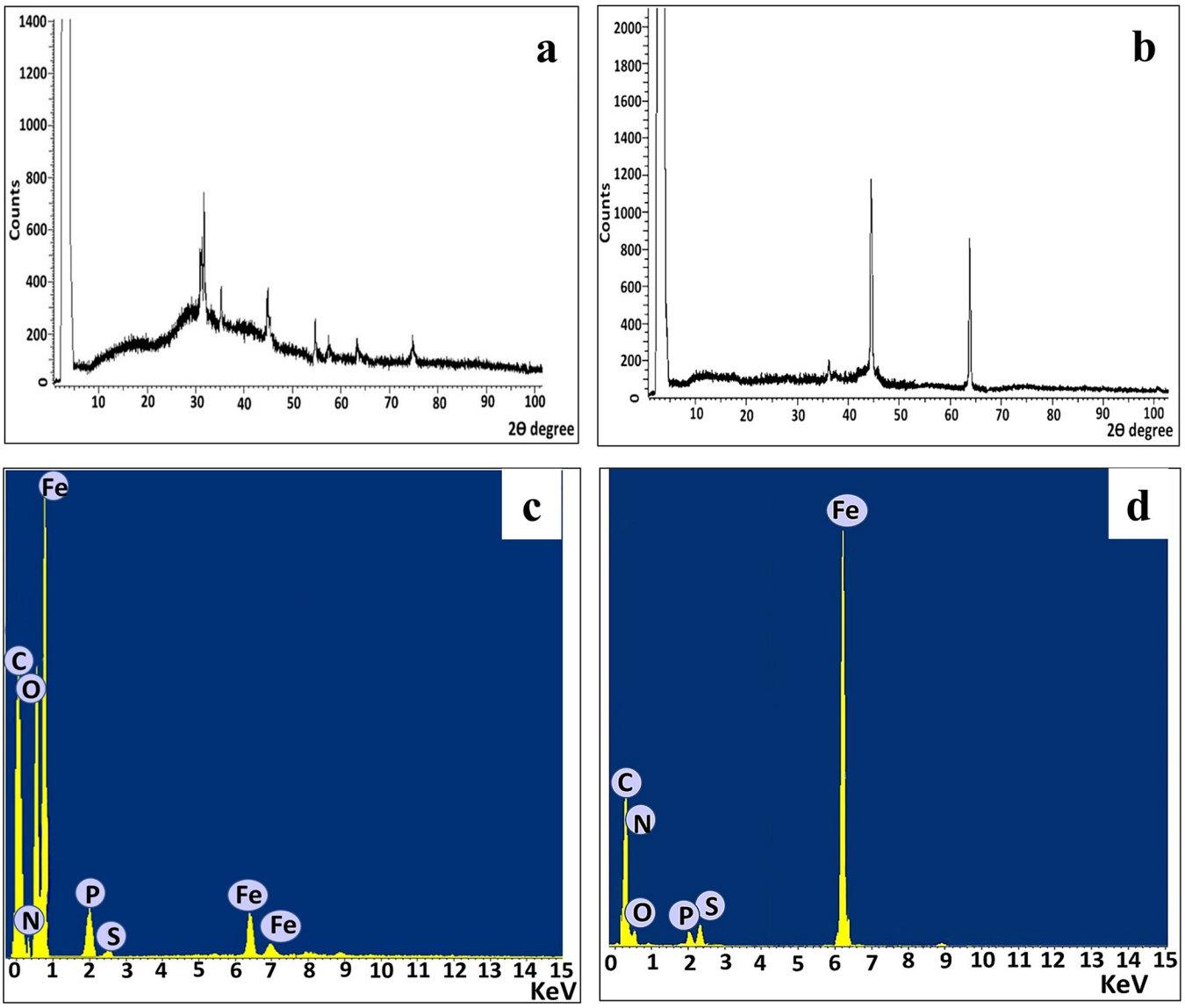

Fig 2. Structural properties of INPs: (a) XRD profile of MNPs; (b) XRD profile of nZVI; (c) EDX pattern of MNPs; (d) EDX pattern of nZVI.

https://doi.org/10.1371/journal.pntd.0011655.g002

are associated to the binding energies of carbon, nitrogen, phosphorous and sulfur, correspondingly with considerable atomic percentages (Fig 2C and 2D). This result agreed with that obtained by Rahman *et al.*, [44] who reported that association of these elements with NPs was routinely observed in green synthesis methods.

I.3. Morphological properties. The microstructure analysis of biogenic INPs, which include morphology, size and their dispersion uniformity, was studied by TEM. The TEM micrographs displayed textural heterogeneity and disparity between MNPs and nZVI; implying the obvious influence of incubation conditions. MNPs that were synthesized aerobically showed numerous, tiny, roughly globular, homogenously distribute with no apparent aggregation and ranged in size from 1.3–11.7 nm (Fig 3A). Whereases, nZVI appeared as large uniform spheres oscillated in their size between 23.5 and 64.4 nm aggregated in nanoclusters (Fig 3B). Such morphological differences between MNPs and nZVI was found previously by

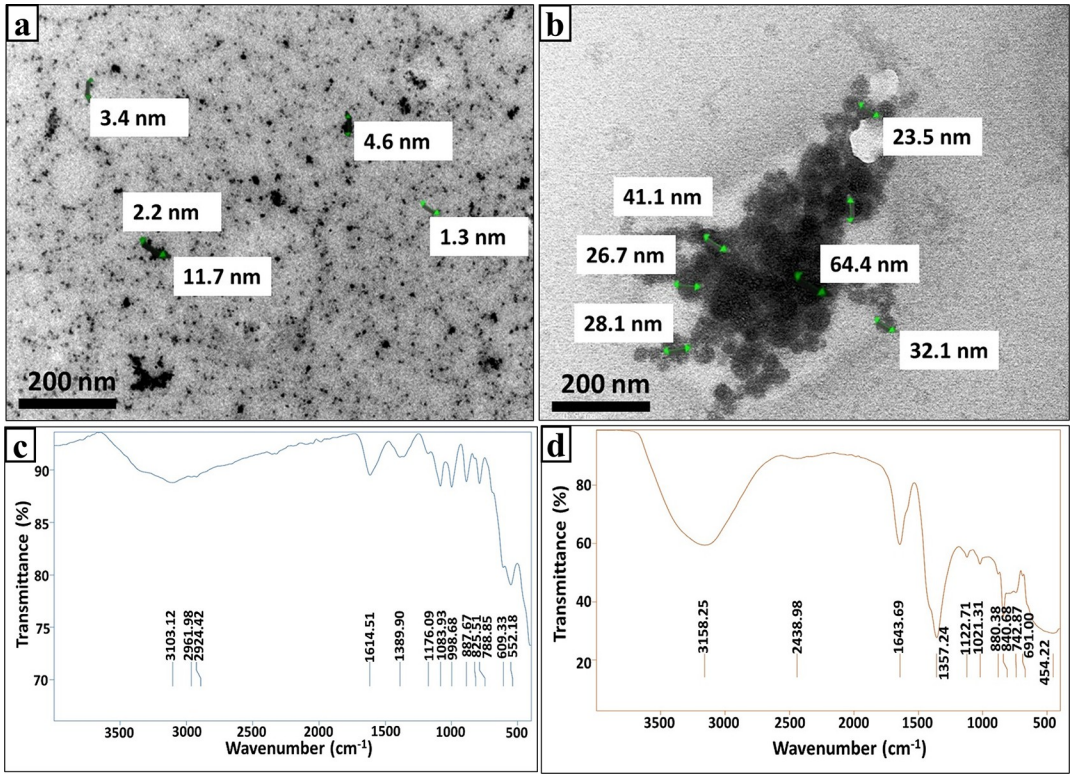

Fig 3. Morphological and functional properties of INPs: (a) TEM of MNPs; (b) TEM of nZVI; (c) FTIR spectrum of MNPs; (d) FTIR spectrum of nZVI.

https://doi.org/10.1371/journal.pntd.0011655.g003

Nadeem *et al.* [45], who assigned that several parameters were involved microbial chemistry, metal type, reaction conditions, interaction mechanism and entire physical state of the reaction.

I.4. Functional properties. As depicted by Fig 3C and 3D the presence of some intensive bands in FTIR patterns of both INPs. Initially, the vibration bands at 3103 and 3158 cm^{-1} were attributed to stretching vibrations of O–H groups of water molecule that was physically adsorbed on INPs [46]. Meanwhile, the wave numbers of 2961 and 2924 cm^{-1} corresponded to the stretching vibration of C-H [47]. Whereas, the bands at 2438 cm^{-1} implied the existence of C = O bonds related to proteins [48]. Besides, the peaks at 1614 and 1643 cm^{-1} are ascribed to amide-I/amide-II linkages, reflecting the conjugation of proteins [47]. The spectral bands at 1357 and 1389 cm^{-1} are assigned to symmetric stretch carboxyl groups (–COOH) [49]. Whereas the bands at 1122 and 1176 cm^{-1} implied the existence of amines C–N [47]. However, the peaks of 1083 and 1021 cm^{-1} could be attributed to the symmetric C–O vibration [41]. The band at 998 cm^{-1} indicated the occurrence of PO_4^{3-} group [50]. Regarding the peaks at 887, 880, 840, 825, 788, 742 cm^{-1}, they could be assigned probably to C-H bending vibrations [51]. Interestingly, the formation of MNPs was confirmed through some distinctive spectral bands such as 552 and 609 cm^{-1}, which are assigned to Fe–O bond in MNPs [41]. Broadly, it is vividly evident the association of Fe with several functional groups, which supported the former results of EDX.

I.5. Particles surface properties. The particle size distribution curve of MNPs denoted that the particle size assessed by 46.82 nm (99.72%) with a standard deviation of 19.02% (Fig 4A), while the hydrodynamic size of nZVI recorded 126.24 nm (89.5%) and 912.1 nm

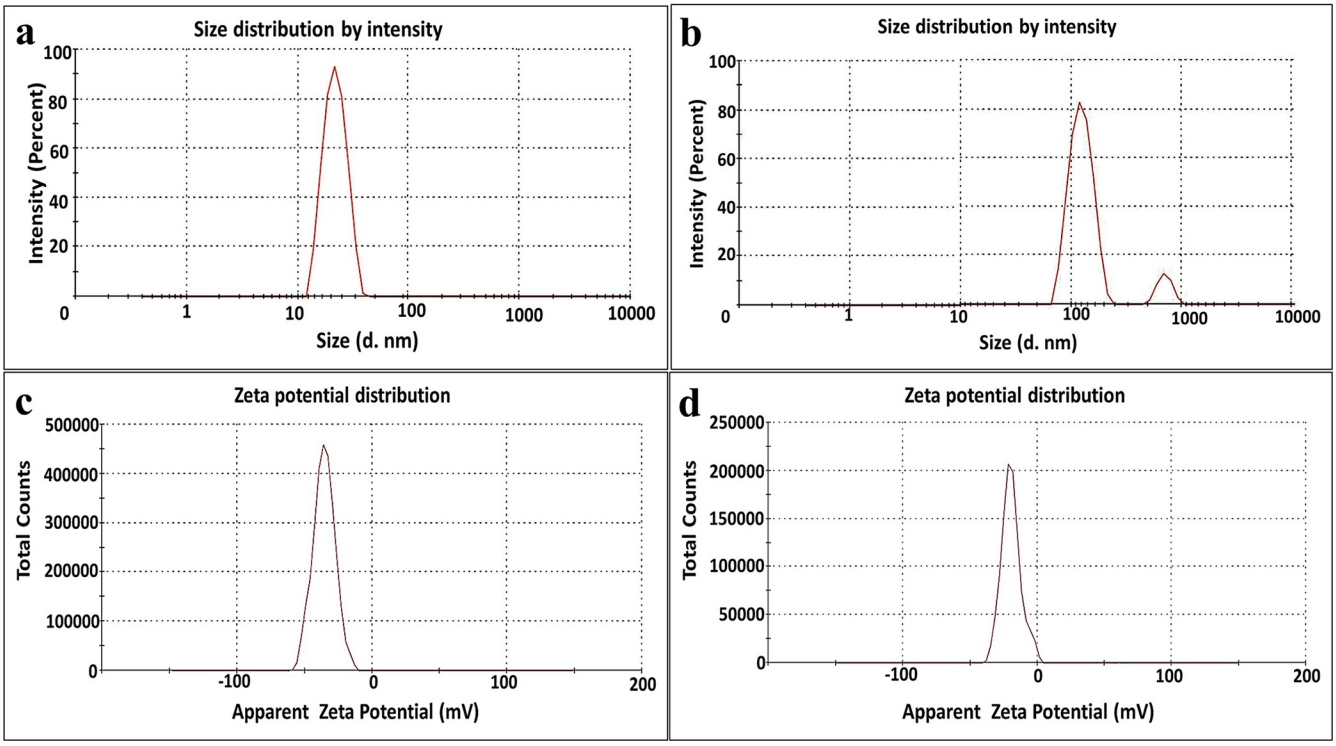

Fig 4. Particle surface properties of INPs: (a) Particle size distribution of MNPs; (b) Particle size distribution of nZVI; (c) Zeta potential of MNPs; (d) Zeta potential of nZVI.

https://doi.org/10.1371/journal.pntd.0011655.g004

(11.5%) with a standard deviation of 20.62% and 9.83%, respectively (Fig 4B). Remarkably, PDI values implied higher monodispersity of smaller MNPs (0.219 nm) in a homogenous distribution than that exhibited by larger nZVI (0.433 nm). Further, ZP of MNPs and nZVI was -35.5 and -20.9 mV, respectively, revealing good and moderate stability of MNPs and nZVI, correspondingly, according to colloid stability ranking based on ZP as stated by Vishwakarma [52]. Notably, the negative sign of ZP pointed out to the existence of negatively charged matrix of bacterial biomolecules [53].

II. Parasitological study

II.1. Mortality rate. There was statistically non-significant difference in mortality rate among all studied subgroups ($P > 0.05$). Death of one mouse was recorded in infected non treated subgroup IIa on the 7th day PI with a mortality rate of 14.28%, whereas no mortalities among mice in other studied subgroups till the sacrifice time (8th day PI) were observed.

II.2. Parasite count. As shown in Table 1, a statistically significant reduction in the mean number of tachyzoites in the peritoneal fluid and liver impression smears was detected in all infected treated subgroups (IIb, IIc and IId) compared to the infected non treated subgroup IIa ($P < 0.001$). Oral administration of MNPs and nZVI to the infected mice resulted in a statistically significant reduction in mean tachyzoite count in peritoneal fluid and liver impression smears (12.83 ± 0.61 and 0.88 ± 0.08) and (99 ± 9.23 and 3.35 ± 0.36) for the two subgroups, respectively, compared to a mean of (403.1 ± 82.54 and 10.82 ± 2.16) for the infected non treated control subgroup ($P < 0.001$). On comparing the effect of MNPs and nZVI with that of SPI on tachyzoite count in peritoneal fluid and liver impression smears, a statistically significant difference was only recorded between nZVI and SPI ($P < 0.001$). While

Table 1. The effect of SPI, MNPs and nZVI on the tachyzoites' burden in peritoneal fluid and liver impression smears of the infected treated subgroups of mice compared to the infected non-treated control.

Subgroup / Tachyzoite count	Non treated (IIa)	SPI-treated (IIb)	MNPs-treated (IIc)	nZVI-treated (IId)	F	p
Peritoneal fluid x10^4						
Median (Min.–Max.)	394 (312–543.5)	29.5 (27.5–30.5)	12.8 (12–13.5)	96.3 (88.5–114)	115.116*	<0.001*
Mean ± SD.	403.1 ± 82.54	29.2 ± 1	12.83 ± 0.61	99 ± 9.23		
%R		**92.76**	**96.82**	**75.44**		
p_0		<0.001*	<0.001*	<0.001*		
Significance		$p_1 = 0.903$, $p_2 = 0.040$*, $p_3 = 0.009$*				
Liver impression smears						
Median (Min.–Max.)	11.3 (7.4–13.4)	1.5 (1.2–1.6)	0.90 (0.80–1.0)	3.4 (2.8–3.7)	105.043*	<0.001*
Mean ± SD.	10.82 ± 2.16	1.45 ± 0.14	0.88 ± 0.08	3.35 ± 0.36		
%R		**86.60**	**91.87**	**69.04**		
p_0		<0.001*	<0.001*	<0.001*		
Significance		$p_1 = 0.807$, $p_2 = 0.033$*, $p_3 = 0.005$*				

% R: Percentage of reduction in each of the studied subgroups relative to infected non treated control

F: F for One way ANOVA test, used in comparison between more than two groups

Post Hoc test (Tukey) is used in pairwise comparisons

p: p value for comparing between the subgroups

p_0: p value for comparing between infected non treated subgroup (IIa) and each other infected treated subgroups

p_1: p value for comparing between SPI-treated subgroup (IIb) and MNPs-treated subgroup (IIc)

p_2: p value for comparing between SPI-treated subgroup (IIb) and nZVI-treated subgroup (IId)

p_3: p value for comparing between MNPs-treated subgroup (IIc) and nZVI-treated subgroup (IId)

*: Statistically significant at $p \leq 0.05$

https://doi.org/10.1371/journal.pntd.0011655.t001

the comparison between the biogenic MNPs and nZVI revealed a statistically significant difference in mean parasite burden in peritoneal fluid and liver impression smears in favour of MNPs ($P < 0.001$).

III. Ultrastructural study

Results of SEM examination are shown in Fig 5. Tachyzoites of mice in the infected non treated subgroup (IIa) appeared generally crescent in shape with completely smooth regular surfaces (Fig 5A and 5B). Whereas treated tachyzoites showed variable surface changes. Most tachyzoites of SPI-treated subgroup (IIb) preserved their crescent shape and the surfaces of most of them were nearly smooth with mild irregularities and few dimples (Fig 5C and 5D). On the other hand, severe and profound morphological changes were detected in tachyzoites of MNPs-treated subgroup (IIc). Most of them appeared shrunken and obviously distorted. Furthermore, the tachyzoite surfaces exhibited marked irregularities with numerous ridges and protrusions. Additionally, noticeable distortion in the apical region was observed in some tachyzoites (Fig 5E and 5F). Comparable but milder surface changes were observed in nZVI-treated subgroup (IId). Despite keeping their crescent shape, some tachyzoites in nZVI-treated subgroup showed surface protrusions and multiple dimples, others showed irregular surface ridges, erosions and distorted posterior end (Fig 5G and 5H).

IV. Immunological and biochemical studies

IV.1. Immunological study. As regards the non infected subgroups, a statistically significant increase in the mean values of serum IFN-γ was recorded in MNPs-treated subgroup (Ic)

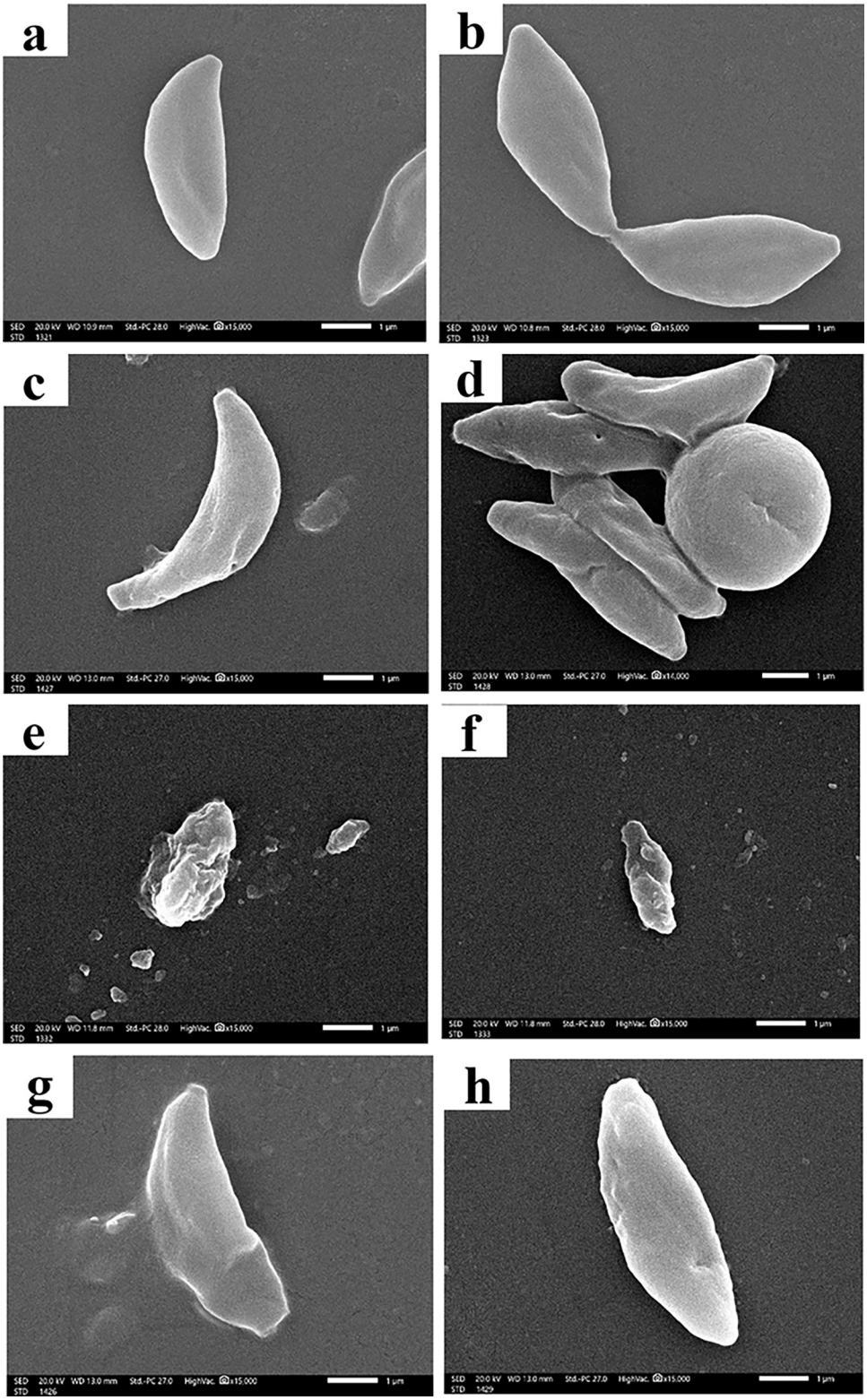

Fig 5. SEM images of *T. gondii* tachyzoites recovered from peritoneal fluid of infected mice: (a & b) Non treated tachyzoites showing typical crescent shape and smooth body with intact regular membrane (x15,000); (c & d) SPI-treated tachyzoites showing minimal changes in the form of mild irregularities and few dimples on the crescent shape surface (x15,000); (e-f) MNPs-treated tachyzoites showed (e) markedly distorted body with multiple deep ridges and

furrows (x15,000); (f) shrunken body and obvious protrusions (x15,000); (g-h) nZVI-treated tachyzoites showed (g) distortion of the posterior end with plasma membrane erosions and ulcerations (x15,000); (h) external protrusions and dimples (x15,000).

https://doi.org/10.1371/journal.pntd.0011655.g005

compared to other subgroups either treated or not. Generally, during the course of infection, the mean levels of INF-γ highly increased in all infected subgroups whether treated or not. The most statistically significant increase in the serum levels of INF-γ among all infected subgroups was only recorded in MNPs-treated infected subgroup (IIc). Whereas the infected subgroups treated with SPI and nZVI showed non-statistically significant difference in the mean levels of INF-γ in comparison with the infected non treated subgroup (Fig 6). Detailed serological results were shown in S1 Table.

IV.2. Biochemical study. *IV.2.1. Oxidative stress*. There was no statistically significant change in sera levels of MDA in non infected treated subgroups (Ib, Ic and Id) in comparison to non infected non treated subgroup (Ia). On the contrary, all infected treated subgroups (IIb, IIc and IId) showed a statistically significant decrease in their serum levels of MDA when compared to the infected non treated subgroup (IIa). The least statistically significant reduction in MDA was noticed in infected nZVI-treated subgroup (IId), followed by infected SPI-treated subgroup (IIb) with slight non-significant difference. While MNPs-treated subgroup achieved a profound statistically significant decrease in MDA in comparison to either SPI-treated or nZVI-treated subgroups (Table 2).

All non-infected treated subgroups (Ib, Ic and Id) revealed no statistically significant difference in the mean sera levels of GSH when compared to non infected non treated subgroup (Ia). On the other hand, there was a statistically significant increase in the mean serum levels of GSH noticed in all infected treated subgroups (IIb, IIc and IId) compared to the infected non treated subgroup (IIa). Meanwhile, there was a pronounced significant increase in GSH observed in MNPs-treated subgroup (IIc) as compared with the other infected treated subgroups (IIb and IId) (Table 3).

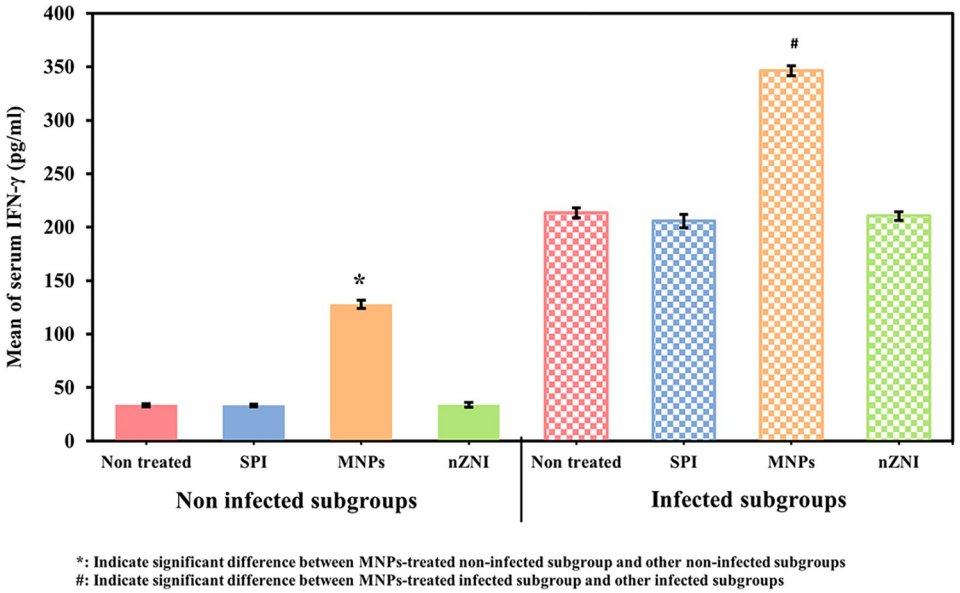

Fig 6. Serum IFN-γ levels among the different studied subgroups.

https://doi.org/10.1371/journal.pntd.0011655.g006

Table 2. The effect of SPI, MNPs and nZVI on the serum MDA level in nmol/ml among all studied subgroups compared to their controls.

		Serum MDA				
Non infected subgroup	**Non treated (Ia)**	**SPI-treated (Ib)**	**MNPs-treated (Ic)**	**nZVI-treated (Id)**	**F**	**p**
Median (Min.–Max.)	6.41 (5.89–6.95)	6.90 (6.25–7.26)	6.50 (6.20–7.31)	6.77 (6.70–7.24)	2.713	0.072
Mean ± SD	6.36 ± 0.41	6.84 ± 0.34	6.61 ± 0.43	6.89 ± 0.23		
Infected subgroup	**Non treated (IIa)**	**SPI-treated (IIb)**	**MNPs-treated (IIc)**	**nZVI-treated (IId)**	**F**	**p**
Median (Min.–Max.)	22.82 (18.99–23.60)	12.69 (11.50–13.15)	7.95 (7.80–8.20)	13.28 (12.13–13.70)	210.893*	<0.001*
Mean ± SD	22.08 ± 1.83	12.56 ± 0.55	7.98± 0.15	13.12 ± 0.54		
p_0		<0.001*	<0.001*	<0.001*		
Significance		p_1<0.001*, p_2 = 0.770, p_3<0.001*				

F: F for One way ANOVA test, used in comparison between more than two groups

Post Hoc test (Tukey) is used in pairwise comparisons

p: p value for comparing between the subgroups

p_0: p value for comparing between infected non treated subgroup (IIa) and each other infected treated subgroups

p_1: p value for comparing between SPI-treated subgroup (IIb) and MNPs-treated subgroup (IIc)

p_2: p value for comparing between SPI-treated subgroup (IIb) and nZVI-treated subgroup (IId)

p_3: p value for comparing between MNPs-treated subgroup (IIc) and nZVI-treated subgroup (IId)

*: Statistically significant at $p \leq 0.05$

https://doi.org/10.1371/journal.pntd.0011655.t002

IV.2.2. Toxicity. Levels of liver enzymes (AST and ALT) and kidney function tests (urea and creatinine) in the sera of non infected mice treated with SPI, MNPs and nZVI did not reveal any statistically significant difference in comparison with the non infected non treated mice (Table 4).

Discussion

Toxoplasmosis is a global health problem caused by the zoonotic parasite, *T. gondii* [2]. The gold standard treatment of toxoplasmosis has recently come under scrutiny because of their

Table 3. The effect of SPI, MNPs and nZVI on the serum GSH level in mg/dl of among all studied subgroups compared to their controls.

		Serum GSH				
Non infected subgroup	**Non treated (Ia)**	**SPI-treated (Ib)**	**MNPs-treated (Ic)**	**nZVI-treated (Id)**	**F**	**p**
Median (Min.–Max.)	2.63 (2.22–2.98)	2.86 (2.65–3.12)	2.67 (2.45–3.10)	2.84 (2.39–3.12)	0.957	0.432
Mean ± SD	2.62 ± 0.26	2.88 ± 0.20	2.73 ± 0.25	2.77 ± 0.33		
Infected subgroup	**Non treated (IIa)**	**SPI-treated (IIb)**	**MNPs-treated (IIc)**	**nZVI-treated (IId)**	**F**	**p**
Median (Min.–Max.)	1.22 (0.98–1.50)	2.51 (2.00–2.85)	8.89 (8.35–9.21)	4.52 (3.95–4.73)	740.935*	<0.001*
Mean ± SD	1.23 ± 0.24	2.44 ± 0.30	8.83 ± 0.30	4.40 ± 0.34		
p_0		<0.001*	<0.001*	<0.001*		
Significance		p_1<0.001*, p_2<0.001*, p_3<0.001*				

F: F for One way ANOVA test, used in comparison between more than two groups

Post Hoc test (Tukey) is used in pairwise comparisons

p: p value for comparing between the subgroups

p_0: p value for comparing between infected non treated subgroup (IIa) and each other infected treated subgroups

p_1: p value for comparing between SPI-treated subgroup (IIb) and MNPs-treated subgroup (IIc)

p_2: p value for comparing between SPI-treated subgroup (IIb) and nZVI-treated subgroup (IId)

p_3: p value for comparing between MNPs-treated subgroup (IIc) and nZVI-treated subgroup (IId)

*: Statistically significant at $p \leq 0.05$

https://doi.org/10.1371/journal.pntd.0011655.t003

Table 4. The effect of SPI, MNPs and nZVI on the level of ALT, AST, urea and creatinine in sera of mice of non infected treated subgroups compared to their non treated control.

Biomarker \ Subgroup	Non treated (Ia)	SPI-treated (Ib)	MNPs-treated (Ic)	nZVI-treated (Id)	F	p
ALT (IU/L)						
Median (Min.–Max.)	26.5 (25–28)	26.2 (24.3–29)	26.8 (24.7–28.5)	27.3 (26.1–30)	0.705	0.560
Mean ± SD	26.54 ± 1.29	26.44 ± 1.58	26.71 ± 1.53	27.53 ± 1.39		
AST (IU/L)						
Median (Min.–Max.)	22.9 (21–25.8)	23.8 (22.3–26.5)	24.3 (20.7–25.6)	24.1 (22.16–27.0)	0.459	0.714
Mean ± SD	23.13 ± 1.84	24.10 ± 1.84	23.76 ± 1.81	24.28 ± 1.81		
Urea (mg/dl)						
Median (Min.–Max.)	14 (10.7–16)	15.5 (11.5–16.5)	13.2 (11–15.7)	14.2 (12.9–17.1)	0.847	0.484
Mean ± SD	13.9 ± 2	14.8 ± 2	13.3 ± 1.6	14.7 ± 1.9		
Creatinine (mg/dl)						
Median (Min.–Max.)	0.70 (0.54–0.88)	0.73 (0.65–0.90)	0.79 (0.57–0.92)	0.70 (0.65–0.95)	0.387	0.763
Mean ± SD	0.70 ± 0.13	0.75 ± 0.09	0.77 ± 0.13	0.75 ± 0.12		

F: F for One way ANOVA test, used in comparison between more than two groups

p: p value for comparing between the subgroups

https://doi.org/10.1371/journal.pntd.0011655.t004

serious adverse effects and emergence of resistant strains [8]. The discovery of safe and effective natural compounds for treatment of *T. gondii* infection seems to be a priority and this is where nanobiotechnology is having a greater chance [54]. Selection of biogenic INPs in the current study was based merely on their unique physicochemical and biological properties (e.g., antimicrobial, antischistosomal activity, etc.), which exceed those fabricated by physicochemical methods [22,25,30]. Herein, the biosynthesis of two types of INPs was successfully fulfilled by the dint of metabolic capability of bionanofactory *Ochrobactrum sp. CNE2*. Via cascade of steps, the biofabrication mechanism fall under the umbrella of oxidation–reduction (redox) reaction. In fact, the nitrate reductase and conjugated electron shuttling molecules may shuttle electrons to the metal ions, leading ultimately to the formation of iron in its nanoform [55]. However, the discripancy in final end product identity could be assigned to the physiological behavior of bacterial cells during growth cycle which express different enzymatic systems in both conditions. Namely, under conditions of oxygen availability, oxide form of INPs were synthesized by the catalysis of periplasmic nitrate reductase [56,57]. On the other hand, in anoxic conditions (i.e., complete absence of oxygen), nZVI was synthesized by the action of respiratory nitrate reductase that enhances the anerobic respiration of nitrate and subsequent generation of the proton motive force [34,41].

Via this bottom-up approach, the biogenic INPs exerted several advantageous features such as; crystalline nature, stability, charge and surface coating [43]. Remarkably, coating the surface of INPs with bacterially-originated functional groups; C = O, C-N, C-H,–OH,–COOH, amide, and PO_4^{3-}, in the same stage of bioreduction, played a vital role in maintaining self-functionalization, stability and facilitating their entry into living cells and bloodstream [34,44]. The negatively charged bacterial matrix biomolecules; sugar-phosphate backbone of nucleic acid residues and amino acids as aspartate and glutamate, act as capping agents that maintain particles functionality and accelerate their interactions with cells [53].

Upon employing both INPs as antitoxoplasmic agents, a potent effectiveness on the tachyzoites was observed as revealed by parasitological and ultrastructural results. However, MNPs possess higher antitoxoplasmic activity than nZVI and SPI evidenced by the highest reduction in count, remarkable shrinkage in size and extensive damage to the surface of tachyzoites. This

can be related to the characteristic physicochemical properties of MNPs such as size, surface area, PDI and ZP. Our findings agreed with Zaki *et al*., [34], who observed that MNPs were more efficient than nZVI in microbial growth suppression in all examined water samples. Similarly, Younis *et al*., [25], reported that MNPs showed privilege over nZVI in reducing adult *S. mansoni* worm burden and liver granulomata number. The smaller MNPs (less than 30 nm) have exponentially more number of atoms on their surface than the larger nZVI which help them bind and cross the membranes, hence take part in subcellular reactions [54]. As documented, the reduction in size of NPs is accompanied by more reactive surface area and subsequently induction of higher amount of reactive oxygen species (ROS) [58]. In addition, the smaller MNPs with high monodispersity (PDI of 0.219) tend to homogenously distribute than larger nonuniform nZVI (with PDI of 0.433). According to colloid stability ranking stated by Vishwakarma *et al*., [52], MNPs with ZP -35.5 mV (higher than ± 30 mV) exhibited better long-term stability than nZVI (-20.9 mV) due to increased electro-static repulsion.

Despite the obvious reduction in parasite burden, SPI showed minimal effect on surface of tachyzoites, supporting earlier observation by Gamea *et al*., [59] who reported minimal surface irregularities of the tachyzoites. This could be attributed to the mechanism of action of SPI, as it binds to the 50S ribosomal subunit, preventing peptide chains elongation, and thus, inhibition of protein synthesis [60].

IFN-γ is the keystone cytokine of the protective cellular immune response against *T. gondii* infection that prevents massive parasitaemia [61]. In the current study, sera IFN-γ levels were obviously increased in noninfected MNPs-treated mice (subgroup Ic) as compared to other noninfected subgroups. Our results were in accordance with Chen *et al*., who reported increased serum IFN-γ level in normal ICR mice IV injected with chemically synthesized MNPs [62]. Noticeably, IFN-γ sera levels were increased following the *Toxoplasma* infection (subgroup IIa). Our results were in accordance with Gaafar *et al*., [10] and Hegazi *et al*., [63] who reported that a strong cellular immune response was elicited by high IFN-γ production during acute and chronic toxoplasmosis, respectively. Although, the IFN-γ production is apparently blocked in the infected cells, rapid growth of the *T. gondii* is contained by a vigorous IFN-γ-dependent immune response by surrounding non infected immune cells [61,64]. However, following oral administration of INPs, the highest sera levels of IFN-γ were achieved by infected mice treated with MNPs (subgroup IIc) as a result of their enhancement of immunity. These results demonstrates that the significant reduction in parasite load and marked ultrastructural changes in tachyzoites in the infected mice treated with MNPs (subgroup IIc) might be linked to the augmentation of the protective IFN-γ-dependent cell-mediated immune response which led to the control of infection.

Determination of MDA and GSH sera levels in *T. gondii* infection is a reliable indicator for follow up and control of treatment [65]. In infected mice of subgroup (IIa), serum MDA was obviously elevated, whereas, antioxidant GSH serum level was markedly decreased. Similarly, Nazarlu *et al*., [66] reported marked increment in MDA and decline in GSH concentration in the serum of rats infected with *T. gondii*. The decrease in GSH, verified that the antioxidant defence system is overwhelmed by the amount of MDA produced in response to the *T. gondii* infection [67].

On the other hand, both INPs markedly decreased MDA and increased GSH sera levels after *T. gondi* challenge (subgroups IIc and IId). Biocompatible INPs is efficiently internalised by tachyzoites, metabolized as the endogenous iron and degraded by hydrolysis into free iron ions which converted the mitochondrial hydrogen peroxide to form a highly reactive hydroxyl radicals via Fenton reaction [68,69]. Such ROS were responsible for the induction of oxidative stress that damaged the protein, DNA, cell membrane and other vital enzymes eventually leading to apoptosis [58]. In addition, oxidative stress could also favor pores formation in the

mitochondria, thus impairing the organelle function [70]. Thus, biogenic nanoscaled iron, MNPs and nZVI, had the potential to be used as antioxidants, by restoration of the GSH level that quenched ROS product, MDA, associated with the *T*. *gondii* infection [71]. MNPs had major potential to undergo oxidation and cause higher levels of antioxidants than nZVI. This could be attributed to their morphology, size, biocompatibility, superparamagnetic, catalytic and biochemical properties [69].

There are concerns on potential nanotoxicity associated with some metal NPs, as silver NPs, even at low concentration and their harmful accumulation in vital organs [72]. The safety of biogenic INPs, MNPs and nZVI, was proved by measuring the liver and renal function biomarkers in serum of mice [73]. These data were consistent with El-Bahr *et al*., [74], who indicated that oral administration of MNPs biosynthesized from *Petroselinum crispum* leaf extract did not induce any hepatic nor renal toxicity in male albino rats. Similarly, Tavakoli *et al*., [75] demonstrated that intraperitoneal injection of nZVI synthesized by *Myrtus communis* did not increase serum level of hepatic enzymes.

Conclusions

Biofabricated INPs, MNPs and nZVI, can serve as highly potent nanotherapeutic agents affording high levels of safety with antitoxoplasmic activity. The promising antitoxoplasmic activity of biogenic INPs appeared to be related to two main interplaying protective mechanisms; immunological, represented by IFN-γ production, and antioxidant mechanisms. Biosynthesized INPs, especially MNPs, may herald a revolution in pharmacological therapy for *T*. *gondii* infections. Further verification of the underlying pharmacodynamics and kinetics of the biosafe MNPs is still needed to be studied.

Supporting information

S1 Table. Supporting data for Fig 6.
(DOCX)

Acknowledgments

We gratefully acknowledge Dr. Fadwa Mostafa Arafa, for her kind cooperation. Our gratitude is further extended to Mrs Dawlat Ahmed for technical assistance with animal experimentation.

Author Contributions

Conceptualization: Nehal Nassef Hezema, Sara Ahmed Abdel Salam.

Data curation: Nehal Nassef Hezema, Sara Ahmed Abdel Salam.

Investigation: Nehal Nassef Hezema, Sara Ahmed Abdel Salam.

Methodology: Nehal Nassef Hezema, Marwa Moustafa Eltarahony, Sara Ahmed Abdel Salam.

Writing – original draft: Nehal Nassef Hezema, Marwa Moustafa Eltarahony, Sara Ahmed Abdel Salam.

Writing – review & editing: Nehal Nassef Hezema, Sara Ahmed Abdel Salam.

References

1. de Barros RAM, Torrecilhas AC, Marciano MAM, Mazuz ML, Pereira-Chioccola VL, Fux B. Toxoplasmosis in Human and Animals Around the World. Diagnosis and Perspectives in the One Health

Approach. Acta tropica. 2022; 231:106432; https://doi.org/10.1016/j.actatropica.2022.106432 PMID: 35390311

2. Calero-Bernal R, Fernández-Escobar M, Katzer F, Su C, Ortega-Mora LM. Unifying Virulence Evaluation in *Toxoplasma gondii*: A Timely Task. Front Cell Infect Microbiol. 2022; 12:868727; https://doi.org/10.3389/fcimb.2022.868727 PMID: 35573788
3. Aguirre AA, Longcore T, Barbieri M, Dabritz H, Hill D, Klein PN, et al. The One Health Approach to Toxoplasmosis: Epidemiology, Control, and Prevention Strategies. EcoHealth. 2019; 16 2:378–90; https://doi.org/10.1007/s10393-019-01405-7 PMID: 30945159
4. Garcia LS, Procop GW. Diagnostic medical parasitology. Manual of Commercial Methods in Clinical Microbiology: International Edition. 2016:284–308.
5. Guglielmi P, Secci D. Treatment of Toxoplasmosis: An Insight on Epigenetic Drugs. Antiprotozoal Drug Development and Delivery: Springer; 2022. p. 293–319.
6. Ben-Harari RR, Goodwin E, Casoy J. Adverse Event Profile of Pyrimethamine-Based Therapy in Toxoplasmosis: A Systematic Review. Drugs in R&D. 2017; 17 4:523–44; https://doi.org/10.1007/s40268-017-0206-8 https://doi.org/10.1007/s40268-017-0206-8. PMID: 28879584
7. Portnoy JM, Pandya A. Drug Allergy. Textbook of Allergy for the Clinician: CRC Press; 2021. p. 387–402.
8. Montazeri M, Mehrzadi S, Sharif M, Sarvi S, Tanzifi A, Aghayan SA, et al. Drug resistance in *Toxoplasma gondii*. Frontiers in microbiology. 2018; 9:2587.
9. Younis SS, Abou-El-Naga IF, Radwan KH. Molluscicidal effect of green synthesized silver nanoparticles using Azadirachta indica on *Biomphalaria alexandrina* snails and *Schistosoma mansoni* cercariae. Asian Pacific Journal of Tropical Biomedicine. 2023; 13 1:35.
10. Gaafar MR, Mady RF, Diab RG, Shalaby TI. Chitosan and silver nanoparticles: Promising anti-toxoplasma agents. Experimental parasitology. 2014; 143:30–8; https://doi.org/10.1016/j.exppara.2014.05.005 PMID: 24852215
11. Adeyemi OS, Murata Y, Sugi T, Kato K. Inorganic nanoparticles kill *Toxoplasma gondii* via changes in redox status and mitochondrial membrane potential. International journal of nanomedicine. 2017; 12:1647–61; https://doi.org/10.2147/ijn.s122178 PMID: 28280332
12. Alajmi RA, Al-Megrin WA, Metwally D, Al-Subaie H, Altamrah N, Barakat AM, et al. Anti-Toxoplasma activity of silver nanoparticles green synthesized with Phoenix dactylifera and Ziziphus spina-christi extracts which inhibits inflammation through liver regulation of cytokines in Balb/c mice. Bioscience reports. 2019; 39 5; https://doi.org/10.1042/BSR20190379 PMID: 30992387
13. Shakibaie M, Ezzatkhah F, Gabal E, Badparva E, Jahanbakhsh S, Mahmoudvand H. Prophylactic effects of biogenic selenium nanoparticles on acute toxoplasmosis: An in vivo study. Annals of Medicine and Surgery. 2020; 54:85–8; https://doi.org/10.1016/j.amsu.2020.04.010 PMID: 32405413
14. Saadatmand M, Al-Awsi GRL, Alanazi AD, Sepahvand A, Shakibaie M, Shojaee S, et al. Green synthesis of zinc nanoparticles using Lavandula angustifolia Vera. Extract by microwave method and its prophylactic effects on *Toxoplasma gondii* infection. Saudi journal of biological sciences. 2021; 28 11:6454–60; https://doi.org/10.1016/j.sjbs.2021.07.007.
15. Albalawi AE, Alanazi AD, Alyousif MS, Sepahvand A, Ebrahimi K, Niazi M, et al. The High Potency of Green Synthesized Copper Nanoparticles to Prevent the *Toxoplasma gondii* Infection in Mice. Acta Parasitologica. 2021; 66 4:1472–9; https://doi.org/10.1007/s11686-021-00421-4 https://doi.org/10.1007/s11686-021-00421-4. PMID: 34050875
16. Phipps O, Al-Hassi HO, Quraishi MN, Kumar A, Brookes MJ. Influence of Iron on the Gut Microbiota in Colorectal Cancer. Nutrients. 2020; 12 9; https://doi.org/10.3390/nu12092512 PMID: 32825236
17. El-Shafey AAM, Hegab MHA, Seliem MME, Barakat AMA, Mostafa NE, Abdel-Maksoud HA, et al. Curcumin@metal organic frameworks nano-composite for treatment of chronic toxoplasmosis. Journal of Materials Science: Materials in Medicine. 2020; 31 11:90; https://doi.org/10.1007/s10856-020-06429-y https://doi.org/10.1007/s10856-020-06429-y. PMID: 33089411
18. Makarov VV, Makarova SS, Love AJ, Sinitsyna OV, Dudnik AO, Yaminsky IV, et al. Biosynthesis of stable iron oxide nanoparticles in aqueous extracts of Hordeum vulgare and Rumex acetosa plants. Langmuir: the ACS journal of surfaces and colloids. 2014; 30 20:5982–8; https://doi.org/10.1021/la5011924 PMID: 24784347
19. Arias SL, Shetty AR, Senpan A, Echeverry-Rendón M, Reece LM, Allain JP. Fabrication of a Functionalized Magnetic Bacterial Nanocellulose with Iron Oxide Nanoparticles. Journal of visualized experiments: JoVE. 2016; 111; https://doi.org/10.3791/52951 PMID: 27285589
20. Montiel Schneider MG, Martín MJ, Otarola J, Vakarelska E, Simeonov V, Lassalle V, et al. Biomedical Applications of Iron Oxide Nanoparticles: Current Insights Progress and Perspectives. Pharmaceutics.

2022; 14 1:204. https://www.mdpi.com/1999-4923/14/1/204. https://doi.org/10.3390/pharmaceutics14010204 PMID: 35057099

21. Revia RA, Zhang M. Magnetite nanoparticles for cancer diagnosis, treatment, and treatment monitoring: recent advances. Materials Today. 2016; 19 3:157–68; https://doi.org/10.1016/j.mattod.2015.08.022 PMID: 27524934

22. Patra JK, Ali MS, Oh I-G, Baek K-H. Proteasome inhibitory, antioxidant, and synergistic antibacterial and anticandidal activity of green biosynthesized magnetic Fe3O4 nanoparticles using the aqueous extract of corn (Zea mays L.) ear leaves. Artificial cells, nanomedicine, and biotechnology. 2017; 45 2:349–56. https://doi.org/10.3109/21691401.2016.1153484 PMID: 26964646

23. Ahmadi S, Fazilati M, Nazem H, Mousavi SM. Green Synthesis of Magnetic Nanoparticles Using Satureja hortensis Essential Oil toward Superior Antibacterial/Fungal and Anticancer Performance. BioMed Research International. 2021; 2021:8822645; https://doi.org/10.1155/2021/8822645 https://doi.org/10.1155/2021/8822645. PMID: 33542927

24. Sathishkumar G, Logeshwaran V, Sarathbabu S, Jha PK, Jeyaraj M, Rajkuberan C, et al. Green synthesis of magnetic Fe3O4 nanoparticles using Couroupita guianensis Aubl. fruit extract for their antibacterial and cytotoxicity activities. Artificial Cells, Nanomedicine, and Biotechnology. 2018; 46 3:589–98; https://doi.org/10.1080/21691401.2017.1332635 https://doi.org/10.1080/21691401.2017.1332635. PMID: 28554257

25. Younis S, Diab R, Eltarahony M, Arafa F. The anti-schistosomal activity of magnetite and zero-valent iron nanoparticles on *Schistosoma mansoni*: An in vivo study. Parasitologists United Journal. 2021; 14 3:269–77.

26. Sevcu A, Cernik M. Oxidative stress in microorganisms exposed to iron nanoparticles. WIT Transactions on Ecology and the Environment. 2010; 141:97–107.

27. Srivastava S, Bhargava A. Applications of Biosynthesized Nanoparticles. In: Srivastava S, Bhargava A, editors. Green Nanoparticles: The Future of Nanobiotechnology. Singapore: Springer Singapore; 2022. p. 285–323.

28. Wu YN, Yang LX, Wang PW, Braet F, Shieh DB. From Microenvironment Remediation to Novel Anti-Cancer Strategy: The Emergence of Zero Valent Iron Nanoparticles. Pharmaceutics. 2022; 14 1; https://doi.org/10.3390/pharmaceutics14010099 PMID: 35056996

29. Hashemi Z, Ebrahimzadeh MA, Biparva P, Mortazavi-Derazkola S, Goli HR, Sadeghian F, et al. Biogenic Silver and Zero-Valent Iron Nanoparticles by Feijoa: Biosynthesis, Characterization, Cytotoxic, Antibacterial and Antioxidant Activities. Anti-cancer agents in medicinal chemistry. 2020; 20 14:1673–87; https://doi.org/10.2174/1871520620666200619165910 PMID: 32560617

30. Chau TP, Brindhadevi K, Krishnan R, Alyousef MA, Almoallim HS, Whangchai N, et al. A novel synthesis, analysis and evaluation of Musa coccinea based zero valent iron nanoparticles for antimicrobial and antioxidant. Environmental Research. 2022; 209:112770; https://doi.org/10.1016/j.envres.2022.112770 PMID: 35063432

31. Johnson AM, McDonald PJ, Neoh SH. Kinetics of the growth of *Toxoplasma gondii* (RH strain) in mice. Int J Parasitol. 1979; 9 1:55–6; https://doi.org/10.1016/0020-7519(79)90066-3 PMID: 447444

32. Eissa MM, Barakat AM, Amer EI, Younis LK. Could miltefosine be used as a therapy for toxoplasmosis? Experimental parasitology. 2015; 157:12–22; https://doi.org/10.1016/j.exppara.2015.06.005 PMID: 26112396

33. Hagras NA, Allam AF, Farag HF, Osman MM, Shalaby TI, Fawzy Hussein Mogahed NM, et al. Successful treatment of acute experimental toxoplasmosis by spiramycin-loaded chitosan nanoparticles. Exp Parasitol. 2019; 204:107717; https://doi.org/10.1016/j.exppara.2019.107717 PMID: 31228418

34. Zaki SA, Eltarahony MM, Abd-El-Haleem DA. Disinfection of water and wastewater by biosynthesized magnetite and zerovalent iron nanoparticles via NAP-NAR enzymes of Proteus mirabilis 10B. Environmental science and pollution research international. 2019; 26 23:23661–78; https://doi.org/10.1007/s11356-019-05479-2 PMID: 31201708

35. Eltarahony M, Zaki S, Abd-El-Haleem D. Concurrent synthesis of zero-and one-dimensional, spherical, rod-, needle-, and wire-shaped CuO nanoparticles by Proteus mirabilis 10B. Journal of Nanomaterials. 2018.

36. El-Zawawy LA, El-Said D, Mossallam SF, Ramadan HS, Younis SS. Triclosan and triclosan-loaded liposomal nanoparticles in the treatment of acute experimental toxoplasmosis. Exp Parasitol. 2015; 149:54–64; https://doi.org/10.1016/j.exppara.2014.12.007 PMID: 25499511

37. Penido MLdO, Nelson DL, Vieira LQ, Coelho PMZ. Schistosomicidal activity of alkylaminooctanethiosulfuric acids. Memórias do Instituto Oswaldo Cruz. 1994; 89:595–602. https://doi.org/10.1590/s0074-02761994000400017 PMID: 8524062

38. Tanaka T, Maeda H, Matsuo T, Boldbattar D, Umemiya-Shirafuji R, Kume A, et al. Parasiticidal activity of Haemaphysalis longicornis longicin P4 peptide against *Toxoplasma gondii*. Peptides. 2012; 34 1:242–50; https://doi.org/10.1016/j.peptides.2011.07.027 PMID: 21849158

39. Chorawala M, Trivedi V, Dave D, Oza P, Shah G. Acute and subacute toxicity studies of cell wall contents of probiotic (*Lactobacillus casei*) in wistar rats and Swiss albino mice. Research Journal of Pharmaceutical, Biological and Chemical Sciences. 2013; 4 2:719–32.

40. Puthukkara ARP, Jose ST, Lal DS. Plant mediated synthesis of zero valent iron nanoparticles and its application in water treatment. Journal of Environmental Chemical Engineering. 2021; 9 1.

41. Mahdavi M, Namvar F, Ahmad MB, Mohamad R. Green biosynthesis and characterization of magnetic iron oxide (Fe_3O_4) nanoparticles using seaweed (Sargassum muticum) aqueous extract. Molecules (Basel, Switzerland). 2013; 18 5:5954–64; https://doi.org/10.3390/molecules18055954 PMID: 23698048

42. Sadek AH, Asker MS, Abdelhamid SA. Bacteriostatic impact of nanoscale zero-valent iron against pathogenic bacteria in the municipal wastewater. Biologia (Bratisl). 2021; 76 9:2785–809; https://doi.org/10.1007/s11756-021-00814-w PMID: 34219748

43. Du J, Chen Z, Ye S, Wiley BJ, Meyer TJ. Copper as a robust and transparent electrocatalyst for water oxidation. Angew Chem Int Ed Engl. 2015; 54 7:2073–8; https://doi.org/10.1002/anie.201408854 PMID: 25581365

44. Rahman SSU, Qureshi MT, Sultana K, Rehman W, Khan MY, Asif MH, et al. Single step growth of iron oxide nanoparticles and their use as glucose biosensor. Results in Physics. 2017; 7:4451–6; https://doi.org/10.1016/j.rinp.2017.11.001.

45. Nadeem A, Naz S, Ali JS, Mannan A, Zia M. Synthesis, characterization and biological activities of monometallic and bimetallic nanoparticles using Mirabilis jalapa leaf extract. Biotechnol Rep (Amst). 2019; 22:e00338; https://doi.org/10.1016/j.btre.2019.e00338 PMID: 31049302

46. Srivind J, Balamurugan S, Usharani K, Prabha D, Suganya M, Nagarethinam V, et al. Visible light irradiated photocatalytic and magnetic properties of Fe-doped SnS 2 nanopowders. Journal of Materials Science: Materials in Electronics. 2018; 29:9016–24.

47. Eltarahony M, Abu-Serie M, Hamad H, Zaki S, Abd-El-Haleem D. Unveiling the role of novel biogenic functionalized CuFe hybrid nanocomposites in boosting anticancer, antimicrobial and biosorption activities. Scientific reports. 2021; 11 1:7790; https://doi.org/10.1038/s41598-021-87363-z PMID: 33833365

48. Ali R, Aslam Z, Shawabkeh RA, Asghar A, Hussein IA. BET, FTIR, and RAMAN characterizations of activated carbon from waste oil fly ash. Turk J Chem. 2020; 44 2:279–95; https://doi.org/10.3906/kim-1909-20 PMID: 33488157

49. Nalbandian L, Patrikiadou E, Zaspalis V, Patrikidou A, Hatzidaki E, N Papandreou C. Magnetic nanoparticles in medical diagnostic applications: synthesis, characterization and proteins conjugation. Current Nanoscience. 2016; 12 4:455–68.

50. Lian S, Diko CS, Yan Y, Li Z, Zhang H, Ma Q, et al. Characterization of biogenic selenium nanoparticles derived from cell-free extracts of a novel yeast Magnusiomyces ingens. 3 Biotech. 2019; 9:1–8.

51. Akyuz S, Akyuz T, Emre G, Gulec A, Basaran S. Pigment analyses of a portrait and paint box of Turkish artist Feyhaman Duran (1886–1970): The EDXRF, FT-IR and micro Raman spectroscopic studies. Spectrochimica Acta Part A: Molecular and Biomolecular Spectroscopy. 2012; 89:74–81. https://doi.org/10.1016/j.saa.2011.12.046 PMID: 22245940

52. Vishwakarma K: Green synthesis of ZnO nanoparticles using Abrus precatorius seeds extract and their characterization. 2013.

53. Zaki S, Etarahony M, Elkady M, Abd-El-Haleem D. The use of bioflocculant and bioflocculant-producing Bacillus mojavensis strain 32A to synthesize silver nanoparticles. Journal of Nanomaterials. 2014;2014.

54. Baby EK, Reji C, M N. Metal-Based Nanoparticles for Infectious Diseases and Therapeutics. 2022. p. 103–24.

55. Wing-ShanáLin I. Biosynthesis of silver nanoparticles from silver (i) reduction by the periplasmic nitrate reductase c-type cytochrome subunit NapC in a silver-resistant E. ácoli. Chemical Science. 2014; 5 8:3144–50.

56. Miot J, Remusat L, Duprat E, Gonzalez A, Pont S, Poinsot M. Fe biomineralization mirrors individual metabolic activity in a nitrate-dependent Fe (II)-oxidizer. Frontiers in microbiology. 2015; 6:879. https://doi.org/10.3389/fmicb.2015.00879 PMID: 26441847

57. Li Y, Katzmann E, Borg S, Schüler D. The periplasmic nitrate reductase Nap is required for anaerobic growth and involved in redox control of magnetite biomineralization in Magnetospirillum gryphiswaldense. Journal of bacteriology. 2012; 194 18:4847–56. https://doi.org/10.1128/JB.00903-12 PMID: 22730130

58. Irshad R, Tahir K, Li B, Ahmad A, A RS, Nazir S. Antibacterial activity of biochemically capped iron oxide nanoparticles: A view towards green chemistry. Journal of photochemistry and photobiology B, Biology. 2017; 170:241–6; https://doi.org/10.1016/j.jphotobiol.2017.04.020 PMID: 28454048

59. Gamea GA, Elmehy DA, Salama AM, Soliman NA, Afifi OK, Elkaliny HH, et al. Direct and indirect anti-parasitic effects of chloroquine against the virulent RH strain of *Toxoplasma gondii*: An experimental study. Acta tropica. 2022; 232:106508; https://doi.org/10.1016/j.actatropica.2022.106508.

60. Chang HR, Pechère JC. Activity of spiramycin against *Toxoplasma gondii* in vitro, in experimental infections and in human infection. J Antimicrob Chemother. 1988; 22 Suppl B:87–92; https://doi.org/10.1093/jac/22.supplement_b.87 PMID: 3182450

61. Sturge CR, Yarovinsky F. Complex immune cell interplay in the gamma interferon response during *Toxoplasma gondii* infection. Infection and immunity. 2014; 82 8:3090–7; https://doi.org/10.1128/iai.01722-14 PMID: 24866795

62. Chen BA, Jin N, Wang J, Ding J, Gao C, Cheng J, et al. The effect of magnetic nanoparticles of Fe(3)O(4) on immune function in normal ICR mice. International journal of nanomedicine. 2010; 5:593–9; https://doi.org/10.2147/ijn.s12162 PMID: 20856834

63. Hegazi A, Toaleb N, El Fadaly H, Abdel-Rahman E, Barakat A. In vivo-cellular and humoral immune response for evaluation of propolis effect on chronic toxoplasmosis in rats. Adv Anim Vet Sci. 2021; 9 7:1045–52.

64. Denkers EY, Kim L, Butcher BA. In the belly of the beast: Subversion of macrophage proinflammatory signalling cascades during *Toxoplasma gondii* infection. Cellular Microbiology. 2003; 5 2:75–83; https://doi.org/10.1046/j.1462-5822.2003.00258.x PMID: 12580944

65. Kiran TR, Karaman U, Arici YK, Yildiz S. Comparison of malondialdehyde, nitric oxide, adenosine deaminase and glutathione levels in patients with *Entamoeba coli*, *Enterobius vermicularis*, *Giardia intestinalis*, *Demodex* spp. positive, hydatid cyst and *Toxoplasma gondii* serum positi. 2019.

66. Nazarlu ZHA, Matini M, Bahmanzadeh M, Foroughi-Parvar F. *Toxoplasma gondii*: A possible inducer of oxidative stress in reproductive system of male rats. Iranian journal of parasitology. 2020; 15 4:521.

67. Gaharwar US, Meena R, Rajamani P. Iron oxide nanoparticles induced cytotoxicity, oxidative stress and DNA damage in lymphocytes. Journal of applied toxicology: JAT. 2017; 37 10:1232–44; https://doi.org/10.1002/jat.3485 PMID: 28585739

68. Nedyalkova M, Donkova B, Romanova J, Tzvetkov G, Madurga S, Simeonov V. Iron oxide nanoparticles—In vivo/in vitro biomedical applications and in silico studies. Advances in colloid and interface science. 2017; 249:192–212; https://doi.org/10.1016/j.cis.2017.05.003 PMID: 28499604

69. Fernández-Bertólez N, Costa C, Brandão F, Teixeira JP, Pásaro E, Valdiglesias V, et al. Toxicological Aspects of Iron Oxide Nanoparticles. In: Louro H, Silva MJ, editors. Nanotoxicology in Safety Assessment of Nanomaterials. Cham: Springer International Publishing; 2022. p. 303–50.

70. Dorostkar R, Ghalavand M, Nazarizadeh A, Tat M, Hashemzadeh MS. Anthelmintic effects of zinc oxide and iron oxide nanoparticles against *Toxocara vitulorum*. International Nano Letters. 2017; 7 2:157–64.

71. Szewczyk-Golec K, Pawłowska M, Wesołowski R, Wróblewski M, Mila-Kierzenkowska C. Oxidative Stress as a Possible Target in the Treatment of Toxoplasmosis: Perspectives and Ambiguities. International journal of molecular sciences. 2021; 22 11; https://doi.org/10.3390/ijms22115705 PMID: 34071892

72. Gudz KY, Matveev AT, Permyakova ES, Bondarev AV, Slukin PV, Ignatov SG, et al. Nanostructured hexagonal BN coating-supported silver and iron oxide nanoparticles and related bactericidal and fungicidal activities. Applied Surface Science. 2022; 603:154418.

73. Keyhani A, Ziaali N, Shakibaie M, Kareshk AT, Shojaee S, Asadi-Shekaari M, et al. Biogenic selenium nanoparticles target chronic toxoplasmosis with minimal cytotoxicity in a mouse model. Journal of medical microbiology. 2020; 69 1:104–10. https://doi.org/10.1099/jmm.0.001111 PMID: 31846412

74. El-Bahr SM, Elbakery AM, El-Gazzar N, Amin AA, Al-Sultan S, Alfattah MA, et al. Biosynthesized Iron Oxide Nanoparticles from Petroselinum crispum Leaf Extract Mitigate Lead-Acetate-Induced Anemia in Male Albino Rats: Hematological, Biochemical and Histopathological Features. Toxics. 2021; 9 6:123. https://www.mdpi.com/2305-6304/9/6/123. https://doi.org/10.3390/toxics9060123 PMID: 34072696

75. Tavakoli S, Sameni F, Ebrahimzadeh MA, Biparva P, Mohammadi H, Zahedi A, et al. Safety Evaluation of Nano Iron Zero Valente Green Synthesized: A Comparative Study. Nanomedicine Research Journal. 2020; 5 2:160–70.